Physica B 580 (2020) 411830

Contents lists available at ScienceDirect

Physica B: Physics of Condensed Matter

journal homepage: http://www.elsevier.com/locate/physb

Structural and optical characterization of novel nitro substituted D-π-A-π-A type chalcone single crystal showing second-order and third-order nonlinear optical properties

Vinay Parol [a], V. Upadhyaya [a,b], Ganesh Shridhar Hegde [a], N.K. Lokanath [c], A.N. Prabhu [a,*]

[a] Department of Physics, Manipal Institute of Technology, Manipal Academy of Higher Education, Manipal, 576104, India
[b] Manipal Centre for Natural Sciences, Manipal Academy of Higher Education, Manipal, 576104, India
[c] Department of Studies in Physics, Manasagangotri, University of Mysore, Mysuru, 570006, India

ARTICLE INFO

Keywords:
Organic material
Chalcone derivative
Single-crystal XRD
Z-scan technique
Second harmonic generation
Two-photon absorption

ABSTRACT

In this report, nonlinear optical crystal has both second-order and third-order nonlinear optical properties, and crystal is grown by using a slow solvent evaporation technique. The functional groups are identified through spectroscopic technique, and crystal structure is obtained from the refinement and analysis of the single crystal elucidated from single-crystal X-ray diffraction study. Furthermore, the study of linear absorbance has been carried out by using UV/VIS/NIR spectroscopic technique. The presence of defect states were analyzed through photoluminescence study. The electronic contribution parameters of the first order and second-order hyperpolarizability have been calculated from the theoretical approach at the DFT level. The second harmonic generation efficiency (SHG) of (2*E*)-1-(3-chlorophenyl)-3-(4-nitrophenyl)prop-2-en-1-one (3CP4NP) has been calculated and compared with the standard material like KDP. Laser damage threshold studies has been performed at 532 nm. Even more, third-order nonlinear optical properties (nonlinear absorption and nonlinear refraction) of 3CP4NP have been carried out from simple and effective Z-scan technique using Q-switched Nd: YAG laser with 532 nm. The optical limiting properties, second-order hyperpolarizability and corresponding third-order nonlinear optical susceptibility of the crystal have been studied in the present investigation.

1. Introduction

During past three decades organic materials have received considerable attention by scientist and engineers due to their synthesis flexibility, ultrafast response, chemical stability and applicability in device performances [1,2]. The organic/inorganic materials are used in several research areas such as nonlinear optical field, electronic devices, advanced photonics technology, laser micro matching, and photolithography and so on [3–5]. Nowadays organic nonlinear optical(NLO) derivatives are gaining importance because one can tune optical property/parameter of the material at the molecular level by optimising charge transfer in the molecule [3]. Those who optimised materials exhibit high optical nonlinearity, and at the same time, organic materials show electronic in origin, which exhibits ultrafast time response depends on the laser pulse width, repetition rate and input intensity [6, 7]. Based on nonlinearity, the organic materials are attempted for many practical applications such as all-optical switching, optical limiting, optical communications, optical data storage, second harmonic generation, electro-optics modulations and so on [8–13]. Among organic materials, chalcones are a type of flavonoids, which are abundant in edible plants. The name chalcone is defined as two aromatic rings attached with the enone group. The chalcones belong to cross-conjugated family, which exhibits high transparency nature, high laser resistance power and ultrafast response time [14–18]. The chalcones have the advantage of being non-toxic, having low cost and easy fabrication. These materials are noteworthy because nonlinear optical absorption property is purely based on two-photon absorption (TPA) and suitable for many practical applications. The optical nonlinearity in this class of material may be due to different mechanical processes such as free carrier absorption, TPA, excited-state absorption (saturable and reverse saturable absorption). NLO properties are very sensitive to the intrinsic defects of the crystals. When the material interacts with high power laser or electron beam, which induce the formation of intrinsic defects that reduces the transparency of the material [19–21]. In the

* Corresponding author. Department of Physics, Manipal Institute of Technology, Manipal, 576104, Karnataka state, India.
E-mail address: ashwatha.prabhu@manipal.edu (A.N. Prabhu).

https://doi.org/10.1016/j.physb.2019.411830
Received 25 September 2019; Received in revised form 23 October 2019; Accepted 26 October 2019
Available online 31 October 2019

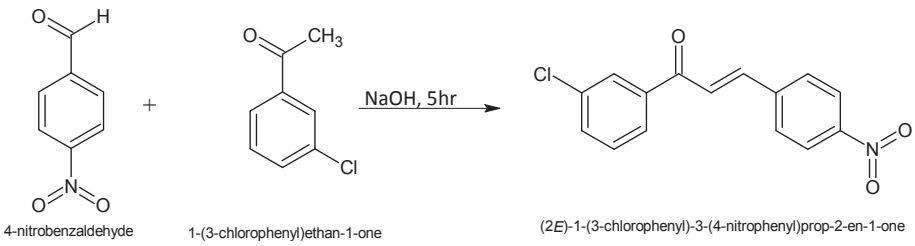

Fig. 1. Synthesis scheme of 3CP4NP.

present investigation, the Z-scan is performed with a low concentration of 3CP4NP in DMF solvent. The solution is completely transparent in the visible to near IR region. As a result, the effect of intrinsic defects in the material is insignificant. Many researchers have reported the third-order NLO study (Z-scan) of chalcone derivatives using a continuous laser beam of 532 nm [22–24]. According to literature, the continuous laser provides a nonlinear thermal effect, which is not suitable for practical applications. The contribution of nonlinearity should be electronic in origin [9,25]. In the present investigation, single beam Q-switched Nd-YAG laser with 532 nm and pulse width 7 ns has been used. In order to avoid thermal nonlinear effect, a low repetition rate (10Hz) is used [26].

Many researchers have been attempted to enhance the TPA coefficient by substituting electron donor/electron acceptor to the aromatic ring, which is attached to the enone group. From the substituted donor electrons, charge transfer takes place to the carbonyl group, which creates a push-pull mechanism in the molecule. As a result, optical nonlinearity could be enhanced. In π-extended chalcone derivatives, the delocalized electrons in the molecule will lead to high TPA coefficient value [27]. Based on this idea, nitro substituted chalcone derivative materials are reported by S. Raghavendra et al. [28] [1-[4-(methylsulfanyl) phenyl]-3-(4-nitrophenyl) prop-2-en-1- one (4MPNP)] and S. R. Prabhu et al. [29] [(2E)-3-(3-methylphenyl)-1-(4-nitrophenyl)prop-2-en-1-one (3MPNP)], by considering benzaldehyde group as nitrophenyl with different ketone group substitutions. Both molecules have centrosymmetric crystal system (second harmonic generation (SHG) efficiency is zero) in fact, these crystals shows better third-order nonlinear response. In addition, Similar type of material [1-(5-bromothiophen-2-yl)-3-(4-nitro-phenyl) prop-2-en-1-one (BTNP)], which exhibits noncentrosymmetric crystal system with SHG efficiency is 4 times that of urea reported by Prabhu et al. [30]. The above molecular design motivated us to synthesize the molecule 3CP4NP by considering nitrophenyl as benzaldehyde group and chlorophenyl as ketone group. The molecular framework with strong acceptor (nitro) and strong donor (chloro) groups has modified the crystal system, which belongs to noncentrosymmetric class. As a result, 3CP4NP shows both second-order and third-order nonlinear response. The nitro and carbonyl groups in the molecule (3CP4NP) under study, act as acceptors (A), and chloro acts as donor (D) group, with a designed molecule having D- π-A- π-A type, which can enhance the thermal stability, laser damage threshold value and third-order nonlinear optical susceptibility.

In the present investigation, nitro based chalcone derivative (3CP4NP) was synthesized, the structure and property were studied for the compound. No reports are available on the study of this molecule. From the theoretical approach, first-order and second-order hyperpolarizability, dipole moment and electronic polarizability were calculated at density functional theory (DFT) level. The grown crystal is characterized by structural properties (FT-IR, and Single-crystal XRD), linear optical properties (UV/VIS/NIR and PL spectroscopy), thermal properties (DSC) and nonlinear optical (second-order and third-order) properties. The results reported in the present investigation could be useful for future laser-assisted applications.

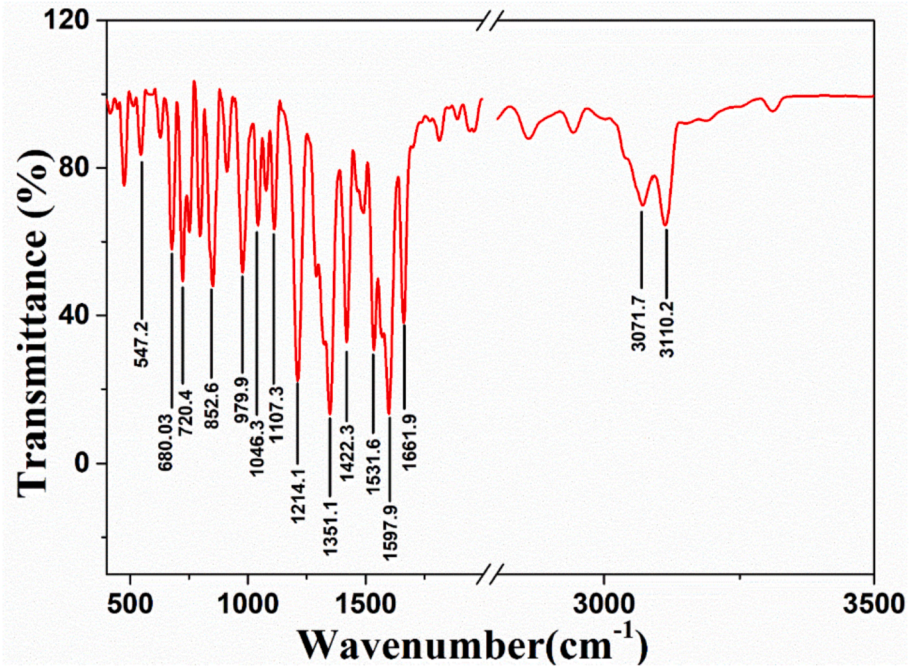

Fig. 2. The FT-IR spectrum of 3CP4NP.

Table 1
Assignment of functional group in FT-IR spectra.

Wave Number (cm^{-1})	Assignments
3110.2, 3071.7	Aromatic C–H stretching vibrations
1661.9	C=O stretching vibrations
1597.9	C=C stretching vibrations
1531.6,1422.3	Aromatic stretching vibrations
1351.1	Symmetry stretching of NO_2 group
1214.1, 1107.3 and 1046.3	In plane bending vibrations
852.6	Aryl C–Cl stretching
720.4, 680.03 and 547.2	Out plane bending vibrations

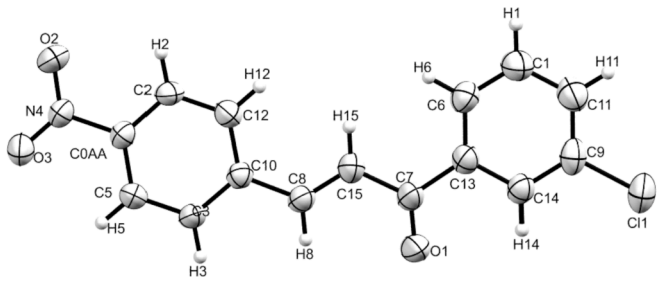

Fig. 3. ORTEP diagram with 50% probability of 3CP4NP.

Table 2
X-ray crystallographic data and refinement factors of 3CP4NP.

CCDC number	**1894859 (3CP4NP)**
Molecular Formula	C_{15} H_{10} O_3 N Cl
Formula Weight	287.69
Temperature (K)	293(2) K
Crystal size	0.24 mm × 0.26 mm × 0.30 mm
Radiation type and wavelength	Mo-K_α and 0.71075 Å
Radiation source	fine-focus sealed tube
Device type	Rigaku XtaLAB Mini X-ray diffractometer
Unit cell dimensions (Å) and Cell angles (°)	
A	6.048(9)
b	5.037(7)
c	21.76(3)
α	90
β	95.865(17)
γ	90
Volume (V)	659.4(16) $Å^3$
Crystal structure, space group	Monoclinic,$P2_1$
Z	2
Total reflection	2152
Observed reflections (I > 2σ(I))	1975
Absorption co-efficient (μ) in (mm^{-1})	0.295
Density (g/cm^3)	1.449
h,k, l	7, −6; 6, −5; 28,−18
Parameters	181
Goodness of fit	1.069
wR_2_all, wR_2_obs.	0.2096,0.1999
R_all, R_obs.	0.0809, 0.0763
$\nabla\rho$(min, max)/e $Å^{-3}$	– 0.388, 0.389

2. Experimental procedure

2.1. Synthesis and single crystal growth

The chalcone derivative was synthesized by Claisen Schmidt condensation reaction method, and required reagents were purchased commercially. The synthesis procedure (Fig. 1) was simple and cost-effective. The compounds of 4 nitrobenzaldehyde (10 mmol) and 3chloroacetophenone (10 mmol), dissolved in methanol solvent, were taken in a round bottom flask. NaOH (10%) was added gradually while the solution was kept for constant stirring for 4 h at room temperature. The reaction progress and compound purity were monitored by thin-layer chromatography.

Furthermore, the compound was added to ice-cold water and kept for 10 h to settle down and precipitate. By using filtration, the product was collected and dried at room temperature for 48 h. The product obtained was purified by repeated recrystallisation in order to grow fine quality single crystals. Here, methanol and DMF (1:1) combination were used for the crystal growth process. Based on solubility, methanol and DMF combination solvent was chosen. The DMF solvent is a slowly evaporating solvent, and the compound is highly soluble in DMF. When DMF was mixed with methanol (1:1), the compound becomes moderately soluble in the mixture. The aforementioned procedure is used to prepare the compound in large quantity (10 gm). The product obtained was taken in 500 ml-beaker and required amount of solvents (methanol and DMF) were added to prepare a saturated solution. The saturated solution was filtered to the 250 ml-beaker to remove small impurities and covered with a perforated sheet. Further, the solution is kept at 35 °C under dust-free atmosphere. After three weeks, fine quality crystals were obtained from the solution.

3. Results and discussions

3.1. FT-IR spectral studies

The peaks obtained in the spectra corresponding to the functional groups were assigned by using FT-IR spectroscopic technique. The spectrum was collected between 400 and 4000 cm^{-1} . The sample was prepared under solid-state method using KBr pellet technique and data obtained from the instrument of PerkinElmer FT-IR spectrometer. Fig. 2 shows the FT-IR spectrum of the 3CP4NP compound and assigned functional groups are shown in Table 1. From Fig. 3, it is observed that, multiplicity band above 3000 cm^{-1} corresponds to the C–H stretching band as compared to aliphatic C–H vibrations. This behaviour is due to reduced negative charges in the carbon atom. The peak at 1661.9 cm^{-1} corresponds to the C=O stretching vibrations. The intense peak in this region is attributed to π-π stacking between carbon and oxygen [31]. It is noteworthy that, C=O group is highly polar due to the double bond. Similarly, the appearance of the peak at 1597.9 cm^{-1} confirms that C=C is conjugated with the C=O group, as a result of which the chalcone derivative of 3CP4NP is formed. The peak pertaining to symmetry stretching of NO_2 group is obtained at 1351.1 cm^{-1}. The in-plane bending vibration peaks appeared between 1500 and 1000 cm^{-1} respectively. It is noted that the in-plane bending vibrations are overlapping with aromatic C–C vibration mode. The wagging vibrations named as out-plane bending vibrations appeared below 1000 cm^{-1}.

3.2. Single-crystal XRD study

A suitably grown crystal was subjected to X-ray diffraction in Rigaku XtaLAB Mini X-ray diffractometer with Mo-K_α radiation at 293(2) K with a wavelength of 0.71075 Å. The data were collected between theta 3.39° and 27.46°, respectively. The following details were used in single-crystal XRD analysis: (1) the data is processed and corrected for the polarization effect by using - SAINT program [32], (2) the crystal structure of 3CP4NP was solved and refined by SHELXTL software [33, 34] and (3) the direct method was applied to locate heavy atoms by using full matrix least square on F^2. This technique is also used to map non-hydrogen atoms anisotropically. The isotropic atoms were positioned geometrically by using riding model. The organic molecules with a better-refined R-factor are allowed up to 10% (R = 0.0763 for 3CP4NP). The unique reflection of 1975 with I > 2σ(I) is used for solving crystal structure and refinement. The molecular structure and its packing diagram were drawn by using mercury software [35].

3CP4NP, the non-centrosymmetric crystal with a formula weight of $C_{15}H_{10}O_3NCl$ belongs to the $P2_1$space group, which corresponds to the monoclinic system. The unit cell parameters are given as a = 6.048(9) Å,

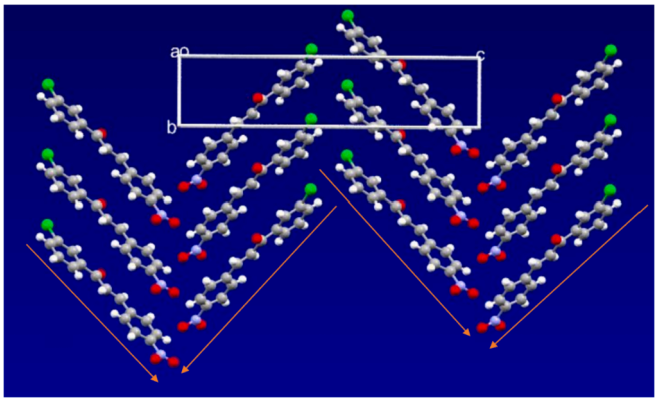

Fig. 4. Parallel molecular packing view along a-axis of 3CP4NP.

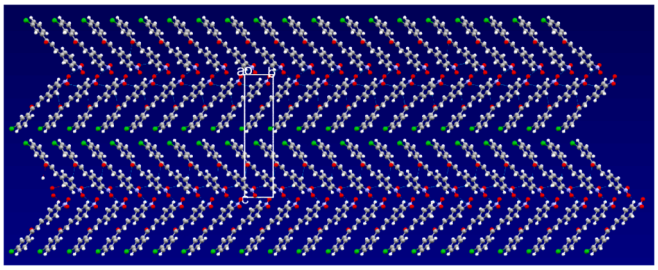

Fig. 5. Intermolecular interactions viewed along a-axis of 3CP4NP.

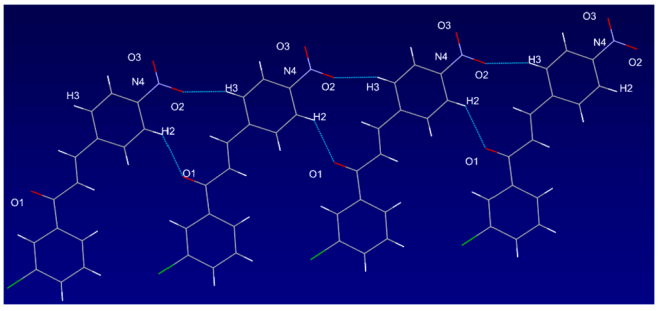

Fig. 6. Hydrogen bond interactions of the molecule 3CP4NP viewed along b-axis.

b = 5.037(7) Å and c = 21.76(3) Å; α = 90°, β = 95.865(17)°, γ = 90° and cell volume is 659.4(16) Å^3 (Table 2). The high electron density due to the presence of electron donor groups makes the molecule highly polarized, as a result, the nonlinear optical property of the molecule gets enhanced. The bond length between C8=C15(-CH=CH-) is 1.322(6)Å and this behaviour confirms that molecule belongs to E-configuration and bond length for 3CP4NP is in good agreement with those in literature [29,36]. The dihedral angle between the aromatic ring of nitrophenyl and chlorophenyl is found to be 3.51°. The small dihedral angle between the aromatic rings suggests that 3CP4NP has planarity. The mean plane angle from the enone group to nitrophenyl ring is about 10.21°. Similarly, the value for the enone group to cholrophenyl ring is 7.17°. The selection of nonlinear optical material based on their molecular design leads to a significant contribution to nonlinear optical efficiency. Figs. 3–5 show the graphical representation of ORTEP diagram, zig-zag movement with parallel molecular packing viewed along a-axis and packing diagram of intermolecular interactions along a-axis of the molecule 3CP4NP. The intermolecular interaction between the molecules attributes to reasonably large complementarity of moderate molecular density in crystal packing. However, the delta-shaped molecules are efficient for second harmonic generation [37]. The C–H···O and C–H … π and π- π stacking interaction tackle the charge transfer process between the molecule and supramolecular domain. The formation of C–H···O and C–H … π bonds explains the ease of obtaining single crystal from the compound 3CP4NP [38]. The interaction of C2–H2···O1 was the reason for stabilizing the crystal packing. The other interaction group elements such as donor electron N4 and donor/-acceptor electrons O2 and O3 interact with the conjugated molecule, which attributes to the π- π stacking interactions. Fig. 6 shows the hydrogen bond interaction and details are enumerated in Table 3. The selected bond length, bond angles, and torsion angles are reported in Table 4. The crystal structure was deposited in the crystallographic data centre with the CCDC number: 1894859.

Table 3
Intermolecular interaction of 3CP4NP.

Interaction	C–H (Å)	H–O (Å)	C–O (Å)	C–H–O (deg)
C2–H2 …. .O1	0.93(1)	2.537(2)	3.221(4)	130.6
C3–H3 …. .O2	0.93(1)	2.490(2)	3.315(2)	147.9

Symmetry: (1) x, y, z; (2) −x, 1/2 + y, −z.

Table 4
Selected bond angle, torsion angle and bond length of 3CP4NP.

Atom Number	Bond Angle (°)	Atom Number	Torsion Angle (°)	Atom Number	Bond Length (Å)
H8–C8–C10	116.7	C2–C0AA-C5-C3	0.5(6)	O1 – C7	1.221 (7)
H8–C8–C15	116.7	C0AA-C2-C12-C10	0.4(6)	O2 – N4	1.237 (5)
Cl1–C9–C14	120.3 (3)	N4–C0AA-C2-C12	178.5(3)	O3– N4	1.212 (5)
C3–C10–C8	118.6 (3)	C2–C0AA-N4-O2	−4.2(5)	C0AA-N4	1.468 (5)
C3–C10–C12	119.3 (4)	C2–C0AA-N4-O3	176.1(4)	C0AA-C5	1.382 (6)
C8–C10–C12	122.1 (3)	C5–C0AA-N4-O2	177.3(3)	C3– C10	1.403 (5)
C6–C13–C7	123.7 (4)	C5–C0AA-N4-O3	−2.4(5)	C7– C13	1.507 (6)
C6–C14–C13	119.1 (4)	C1–C6–C13–C7	175.7(4)	C7– C15	1.476 (6)
C7–C13–C14	117.1 (4)	C1–C6–C13–C14	0.5(7)	C8– H8	0.93
C9–C14–C13	119.6 (4)	O1–C7–C13–C6	171.0(5)	C8– C10	1.483 (6)
C7–C15–C8	121.5 (4)	O1–C7–C13–C14	−5.3(6)	C8– C15	1.322 (6)
C0AA-C5-C3	118.6 (4)	C15–C7–C13–C6	−7.6(6)	C15–H15	0.931
C0AA-C5-H5	120.7	C15–C7–C13–C14	176.1(4)		
C1–C6–C13	120.9 (4)	O1–C7–C15–C8	3.8(7)		
O1–C7–C13	119.3 (4)	O1–C7–C15–H15	−176.1		
O1–C7–C15	121.4 (4)	C13–C7–C15–C8	177.6(4)		
C2– C0AA-N4	118.9 (3)	C15–C8–C10–C3	173.8(4)		
C2– C0AA- C5	122.3 (3)	C15–C8–C10–C12	6.6(7)		
N4– C0AA-C5	118.7 (3)	H8–C8–C15–H15	−177.4		
H3–C3–C10	119.6	C10–C8–C15–C7	177.4(4)		
C5–C3–C10	120.7 (4)	Cl1–C9–C11–C1	179.4(4)		
O2–N4–O3	123.6 (3)	Cl1–C9–C14–C13	179.6(3)		
O2–N4–C0AA	117.3 (3)	C11–C9–C14–C13	0.7(7)		
O3–N4–C0AA	119.1 (3)	C8–C10–C12–C2	178.6(4)		

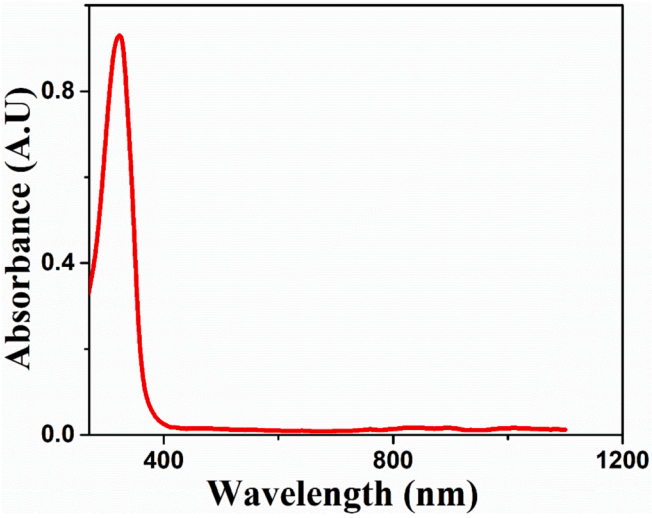

Fig. 7. UV/VIS/NIR spectrum of 3CP4NP.

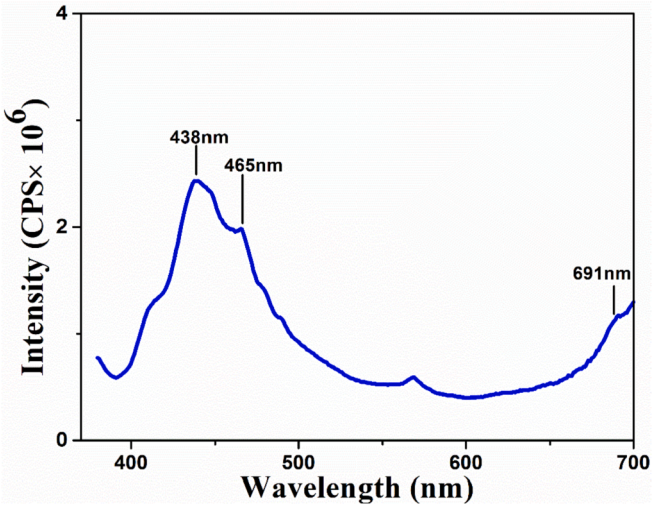

Fig. 8. PL spectrum of 3CP4NP.

3.3. Linear optical properties

The UV-VIS-NIR spectrum of the material was recorded from SHIMADZU UV-1800 spectrometer in order to get the information about the types of electronic transition, localized states, and electronic band structures. The spectra was collected between 190 and 1100 nm in solution form, and DMF solvent was chosen. Fig. 7 shows a prominent absorption characteristic behaviour for 3CP4NP in DMF solvent. The maximum absorbance is found to be 321 nm, which corresponds to the transition of π- π* or n- π* from the unsaturated carbonyl group [39]. The entire transparency was found in the VIS and NIR region with a cut-off wavelength of 369 nm. The entire transparency behaviour in the visible and near-IR region shows that material is efficient for NLO device applications.

3.4. Photoluminescence (PL) studies

PL spectrum was taken from the spectrometer FluoroMax-4CP between 380 nm and 700 nm. The defect states were identified by using a nondestructive technique, and PL emission spectra were collected with an excitation wavelength of 360 nm. The defects states were observed in the visible region and the corresponding wavelengths are given as

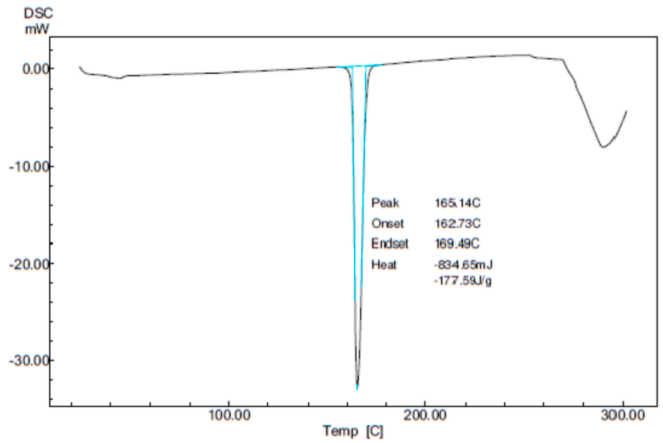

Fig. 9. DSC plot of 3CP4NP.

Table 5
DSC data of some organic NLO materials.

Crystal	Melting Point (°C)
(2*E*)-1-(3-chlorophenyl)-3-(4-nitrophenyl)prop-2-en-1-one	**165 [present study]**
1-(5-bromothiophen-2-yl)-3-(4-nitro- phenyl)prop-2-en-1-one	201.8 [30]
(2E)-3-(3-methylphenyl)-1-(4-nitrophenyl)prop-2-en-1-one	122 [29]
1-(3, 4-dimethylphenyl)-3-[4(methylsulfa-nyl) phenyl] prop-2-en-1-one (4DPMS)	106 [42]
3-(4-fluorophenyl)-1-(4-methoxyphenyl)-prop-2-en-1-one)	118 [43]
3-(3-fluorophenyl)-1-[4-(methylsulfanyl) phenyl] prop-2-en-1-one (FMP)	96 [44]
4-[(1*E*)-3-(5-chlorothiophen-2-yl)-3-oxoprop-1-en-1-yl] phenyl4-methylbenzene-1-sulfonate	115 [45]

438 nm, 465 nm and 691 nm. Fig. 8 shows, the major sharp peak corresponding to the defect states in the violet region at 438 nm and another small peak in the blue region at 465 nm corresponding to defects states for blue light emission property. The several transitions were involved in the widespread behaviour between 404 nm and 500 nm. This widespread behaviour in the material is due to the contribution of electron donor/electron acceptor groups in the aromatic ring, which leads to charge transfer between the aromatic rings [40,41]. The presence of another defect state at 691 nm, is attributed to corresponding light (red) emission property.

3.5. Thermal studies

The thermal property has been analyzed by using a differential scanning calorimeter (DSC) technique in order to know the melting point (M.P.) of the material. The sample of 5 mg was taken in a crucible and temperature is varied between 25 and 300°*C* under nitrogen atmosphere at 10°*C*/min. The spectrum is collected by using SHIMADZU DSC-60 plus. Fig. 9 shows the spectra of the DSC plot, by measuring heat flow with respect to temperature. The first endothermic peak corresponding to the melting point of 3CP4NP, is obtained in the vicinity of 165°*C*. There is no phase transition below this temperature and the material has good crystallite behaviour and purity. It is noteworthy that, the presence of the nitro group in the molecule makes the crystal thermally stable; moreover, the result was compared with that of other chalcone derivatives. The p-nitro substituted chalcone derivatives have shown higher melting point [29,30]. The other group elements such as methoxy, methyl sulfanyl and thiophene substituted chalcone derivatives show low melting point as compared to nitro substituted chalcone derivatives [42–46] as shown in Table 5. The thermally stable organic materials (M.P. above 150°*C*) are more suitable for device applications.

Table 6
Electronic contribution parameters of 3CP4NP.

Electronic contribution parameters	3CP4NP	Electronic contribution parameters	3CP4NP	Electronic contribution parameters	3CP4NP
μ	3.59	α	35.81	β_{yzz}	6.43
μ_x	−1.35	$\Delta\alpha$	52.84	β_{zzz}	−6.52
μ_y	−1.47	β_{xxx}	−0.88	β_{tot}	18.65
μ_z	2.98	β_{xxy}	1.03	γ_{xxxx}	−122.5
α_{xx}	30.04	β_{xyy}	−1.44	γ_{yyyy}	77.00
α_{yy}	39.42	β_{yyy}	5.60	γ_{zzzz}	45.54
α_{zz}	37.98	β_{xxz}	−0.85	γ_{xxyy}	−73.52
α_{xy}	−8.89	β_{xyz}	0.57	γ_{xxzz}	1.83
α_{xz}	0.76	β_{yyz}	−5.73	γ_{yyzz}	3.38
α_{yz}	−20.96	β_{xzz}	−0.07	γ_{tot}	−27.32

3.6. Electronic contributions: NLO activity

To understand the structure-property relation of the material, the theoretical calculation is necessary. The theoretical calculation is done by quantum chemistry program. The calculation of 3CP4NP was performed by using Gaussian09 package software [46] (B3LYP/6-311++G (d.p)) [47,48] at DFT level. The nonlinear parameters were calculated by using finite field method. The electronic structure parameters such as dipole moment (μ), anisotropic polarizability ($\Delta\alpha$) and hyperpolarizability parameters (first order (β) and second-order(γ)) expressed in terms of Taylor expansion is given by,

$$E = E^0 - \sum_i \mu_i F^i - \frac{1}{2}\sum_{ij}\alpha_{ij} F^i F^j - \frac{1}{6}\sum_{ijk}\beta_{ijk}F^i F^j F^k - \frac{1}{24}\sum_{ijkl}\gamma_{ijkl} F^i F^j F^k F^l + \ldots$$

The total dipole moment (μ_{tot}), anisotropy of polarizability ($\Delta\alpha$), first order hyperpolarizability (β) and second order hyperpolarizability(γ) were calculated from the following relations,

$$\mu_{tot} = \sqrt{\mu_x^2 + \mu_y^2 + \mu_z^2}$$

$$\Delta\alpha = \frac{1}{\sqrt{2}}\sqrt{(\alpha_{xx} - \alpha_{yy})^2 + (\alpha_{yy} - \alpha_{zz})^2 + (\alpha_{zz} - \alpha_{xx})^2 + 6\alpha_{xy}^2 + 6\alpha_{yz}^2 + 6\alpha_{zx}^2}$$

$$\beta_{ele} = \sqrt{(\beta_{xxx} + \beta_{xyy} + \beta_{xzz})^2 + (\beta_{yyy} + \beta_{yzz} + \beta_{yxx})^2 + (\beta_{zzz} + \beta_{zxx} + \beta_{zyy})^2}$$

$$\gamma_{ele} = \frac{1}{5}\left[\gamma_{xxxx} + \gamma_{yyyy} + \gamma_{zzzz} + 2(\gamma_{xxyy} + \gamma_{xxzz} + \gamma_{yyzz})\right]$$

where μ_{tot} represented in terms of Debye, polarizability (α and $\Delta\alpha$) in $10^{-24}esu$ and hyperpolarizability parameters corresponding to first order and second order are in $10^{-30}esu$ and $10^{-40}esu$ respectively.

The first order hyperpolarizability parameters were expressed in terms of third rank tensor matrix $3 \times 3 \times 3$, respectively. Based on Kleinman symmetry relations [49], the components were reduced to 10 from 27. Table 6 shows all the electronic contribution parameters of the 3CP4NP molecule. From the calculation, it is noted that z-component corresponding to the dipole moment $\mu_z = 2.98$ Debye has large value then x and y components and total dipole moment was obtained as $\mu = 3.59$ Debye. In electronic components, the dipole moment and polarizability parameters are inter-dependent therefore, the values of average polarizability and anisotropic polarizability were found to be $35.81 \times 10^{-24}esu$ and $52.84 \times 10^{-24}esu$ respectively. The maximum polarizability is in the y-direction ($\alpha_{yy} = 39.42 \times 10^{-24}esu$) due to delocalization of electron. The first order hyperpolarizability for 3CP4NP is about $18.65 \times 10^{-30}esu$, which is almost 48.3 times that of urea (3.728×10^{-31} esu)[50]. The β_{zzz} exhibits high value ($\beta_{zzz} = -6.52 \times 10^{-30}esu$), compared with other two components. Therefore, the charge transfer takes place through a π-conjugation bridge along z-direction. This process is involved by intermolecular charge transfer. Furthermore, the third-order nonlinear optical properties were expressed by electronic contribution of second-order hyperpolarizability(γ_{ele}). The total value of γ_{ele} was found to be $-27.32 \times 10^{-40}esu$. However, the value of γ is negative due to self-defocusing effect, based on the theory of third-order nonlinearity. It is noteworthy that, negative γ materials exhibit extraordinary performance in system controlling and show large amount of responsiveness by small variation in molecular structure [51].

3.7. Laser damage threshold (LDT) study

In the present study, surface damage threshold experiment is performed to confirm the withstand capability of the crystal with high power laser. Here we consider, flat and polished surface crystal (thickness 1.2 mm) mounted on a holder and focused with an Nd:YAG laser beam of 532 nm (pulse width and repetition rate are 6 ns and 10Hz respectively). The output intensity is controlled by filters and sample is placed at the focal point of a converging lens (focal length = 4 cm). Furthermore, the energy parameter is varied until the crystal surface gets damaged. The surface damage value is calculated by using energy (1.6 mJ) parameter and represented in terms of power density (P_d) and is given by,

$$(P_d) = \frac{E}{\tau\pi r^2}\,\mathrm{GW}\Big/\mathrm{cm}^2$$

where, r is the beam spot size = 3.4 mm and τ is the laser pulse width. The LDT value of 3CP4NP is found to be 7.34 GW/cm^2.

3.8. Nonlinear optical properties

3.8.1. Second-harmonic generation studies

The grown crystal of 3CP4NP was taken in powder form for SHG measurement by using Kurtz and Perry technique [52]. The homogenous particles of 3CP4NP crystal were filled in the capillary tube. The laser beam of 1064 nm was focused on the sample with a pulse width of 10 ns and energy 1.2 mJ/pulse. The fundamental beam was focused through the lens on to the sample and output intensity was filtered to remove fundamental beam using IR filters.

Furthermore, the SHG signal was collected by using Hamamatsu-R 2059 photomultiplier tube detector and were converted into an electric signal and fed to Tektronix-TDS 3052B oscilloscope. The uniform powder crystalline samples with particle size of 130–160μm has been taken for both 3CP4NP and KDP crystal. Under the same condition, the amplitude signal voltage for KDP was measured and found to be 22 mV. Similarly, for 3CP4NP, the amplitude signal was about 4 mV. From the result, SHG efficiency for 3CP4NP 0.2 times less than that of KDP crystal. The molecular orientation and effective charge transfer at a particular axis was the main reason for low SHG efficiency [37]. In order to enhance SHG efficiency, the donor electron (chloro) must be chosen in a para position instead of meta position. Despite that, in the selection of nonlinear optical materials for SHG applications, care must be taken in terms of molecular orientations.

3.8.2. Third-order nonlinear optical studies

The nonlinear absorption, sign and magnitude of the nonlinear refractive index were assessed by using open/closed aperture Z-scan technique developed by Sheik-Bahae [53,54]. This technique gained rapid acceptance in the field of nonlinear optics due to its simplicity and as a standard technique. An Nd:YAG laser source operated at 532 nm (pulse width of 7 ns and repetition rate of 10 Hz) was focused using lens of focal length of 200 mm into the cuvette containing solution. The probing beam in the Z-scan measurements is a Gaussian with TEM_{00} fundamental mode. The laser beam is focused through a lens and aligned

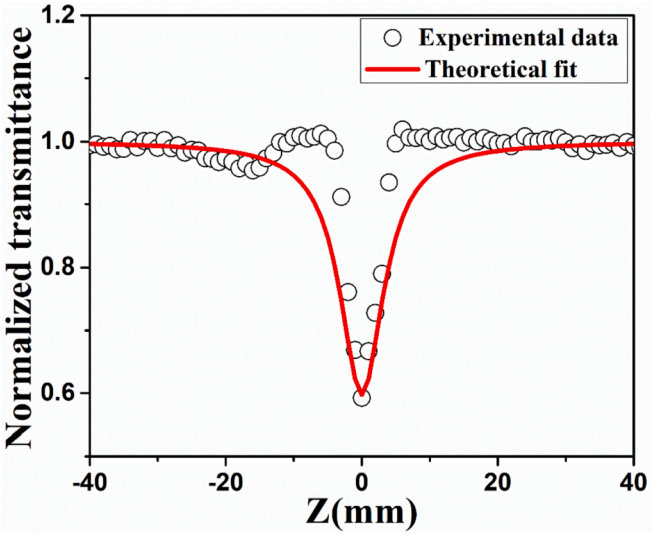

Fig. 10. Open aperture Z-scan data with 2 PA model of 3CP4NP.

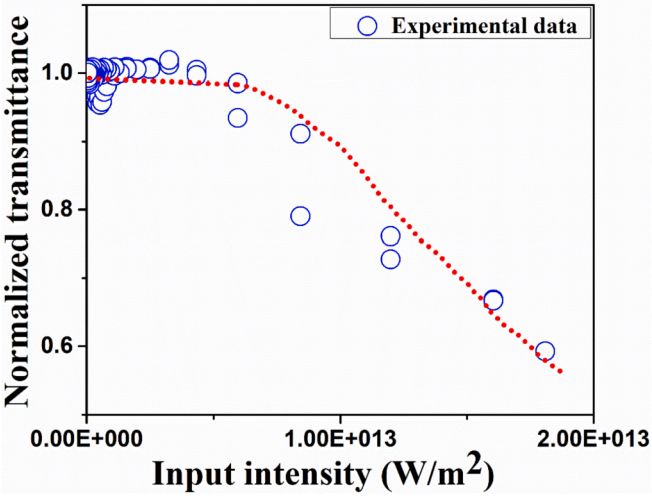

Fig. 11. Optical limiting curve of 3CP4NP.

in the straight line as a result beam follows Gaussian intensity distribution. As the beam focused with a focal point (Z = 0) then maximum intensity is obtained.

Moreover, the NLO properties are intensity-dependent and perfect Gaussian beam profile will provide significant result in third-order NLO properties. The range that nonlinearity change in the material depends on the Rayleigh range, which in turn depends on beam diameter at the entrance of the focusing lens and incident wavelength. For 3CP4NP, Rayleigh range is calculated to be 2.8 mm, which is greater than the thickness of the sample.

The laser beam is focused onto the quartz cuvette of 1 mm thickness and photodetector is placed in the far-field to collect the transmitted intensity obtained from the sample. The pulse train signal data were acquired from the attached computer. The laser beam waist of the radius (ω_0) is 21.8 μm. The nonlinear absorption (saturable or reverse saturable absorption) behaviour in the material depends on the pulse width and laser excitation wavelength. The nonlinear process involved by many absorption mechanisms such as two-photon absorption (TPA), free carrier absorption (FCA), excited-state absorption so on.

In open aperture Z-scan, the intensity is collected from the detector with translating movement from +Z to –Z position and the nonlinear absorption coefficient are calculated at the focus (Z = 0). In order to

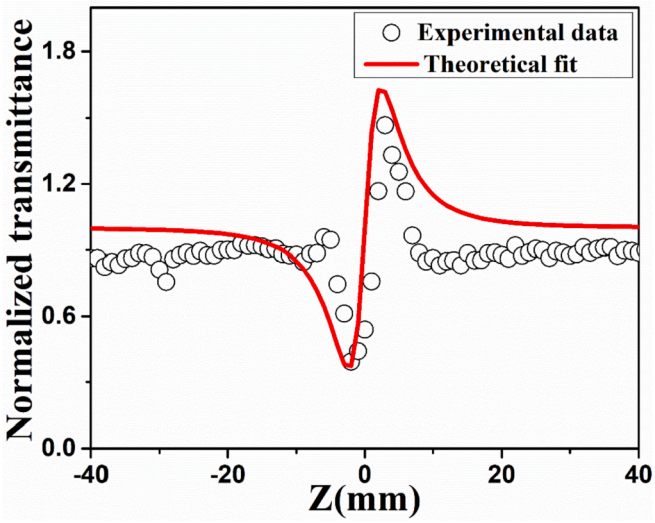

Fig. 12. Closed/open aperture Z-scan data of 3CP4NP.

confirm the mechanism, TPA model is applied and is shown in Fig. 10. The theoretical model fits with the experimental data, which confirm that nonlinearity is associated with two-photon absorption. The Gaussian pulse with an incident Gaussian spatial profile is applied for on-axis sample position. The two-photon model is applied to on scale nonlinear transmittance data

$$T(z) = 1 - \frac{1}{2\sqrt{2}}\beta I_o L_{eff}\frac{1}{1+\frac{z^2}{z_0^2}}$$

where L_{eff} is the effective length (thickness), I_o is the intensity at Z = 0 position and $Z_0 = \frac{\pi\omega_0^2}{\lambda}$.

The value of nonlinear absorption coefficient was calculated from the two-photon model fit, and the value of β was found to be 6.37 cm/GW at $I_o = 1.81$ GW/cm^2.

Fig. 11 shows, optical limiting (OL) behaviour of 3CP4NP sample, and data were extracted from the open aperture Z-scan results. The behaviour of OL shows the reverse saturable absorption and the curve is saturated up to a certain point, which is identified as the threshold point. The limiting threshold value of 3CP4NP is found to be 0.59 GW/cm^2.

The nonlinear refractive index is calculated from the closed aperture Z-scan technique. The behaviour of valley-peak shows the positive refractive index, as shown in Fig. 12. The nonlinear refractive index is calculated by,

$$n_2(\text{esu}) = \left(cn_0/40\pi\right)\gamma\left(\text{m}^2/\text{W}\right)$$

where γ is the nonlinear refraction coefficient ($\gamma = \frac{\Delta\varphi_0\lambda}{2\pi L_{eff} I_0} = 1.553 \times 10^{-17}$ m^2/W)

The normalised transmittance equation for closed aperture is given by,

$$T(Z) = 1 - \frac{4X\Delta\varphi_0}{(X^2+9)(X^2+1)}$$

where, $\Delta\varphi_0$ is the nonlinear phase shift ($\Delta\varphi_0 = \frac{\Delta T_{P-V}}{0.406(1-S)^{0.25}}$ with $S = 50\%$).

The second-order molecular hyperpolarizability (γ_h) and third order nonlinear susceptibility were calculated from the following relations,

$$\gamma_h = \frac{\chi^{(3)}}{N_c L^4}$$

Table 7
Third-order nonlinear optical parameters of some chalcone derivatives measured by using nanosecond laser (532 nm).

Sample	wavelength	n_2(esu) × 10^{-11}	β(cm/GW)	$Re(\chi^{(3)})$(esu) × 10^{-12}	Im($\chi^{(3)}$)(esu) × 10^{-12}	$\chi^{(3)}$(esu) × 10^{-12}
3CP4NP [present study]	532 nm 10Hz	5.489	6.37	8.62	1.5	8.74
CTDMP [55]	532 nm 10Hz	1.532	3.057	0.164	0.047	0.17
FMOC-3 [56]	532 nm	− 0.496 − 1.779	0.965	1.56	1.31	2.03
FMOC-7 [56]	10Hz		3.75	5.62	5.1	7.58
4-Methoxy	532 nm	−2.44	6.27	0.26	0.097	0.280
C3 [57]	10Hz	−1.502	2.65	0.161	0.041	0.166
C4 [57]						
DMMC [59]	800 nm, 80 MHz	− 2.75	1.7	6.62	0.93	6.68
Terphenyl derivatives [58]	532 nm	− 1.148	1.489	− 0.1230	0.0228	0.125
S1	10Hz	− 1.185	2.025	− 0.1270	0.0312	0.31
S2		− 1.787	2.352	− 0.19140	0.0362	0.194
S3		− 2.006	5.206	− 0.2149	0.0801	0.229
S4						
1,5-Diaminoanthraquinone [60]	532 nm 10Hz	–	11.36	6.2075	3.7669	7.2609
Charge transfer complexes [61]	532 nm 10Hz	5.45	73	–	–	24
PTZ-I_2						

$$\chi^{(3)} = \sqrt{(Re(\chi^{(3)})^2 + \left(Im(\chi^{(3)})\right)^2}$$

The real part of third-order nonlinear susceptibility depends on nonlinear refractive index value whereas, the imaginary part based on nonlinear absorption coefficient parameter. Similarly, the value of second-order hyperpolarizability affects $\chi^{(3)}$ because, delocalization of π-electron makes the charge distribution in the aromatic ring, as a result,γ_h has been enhanced to a higher value. The value of second-order molecular hyperpolarizability is found to be 3.82×10^{-30}esu and the value of third-order nonlinear susceptibility is 0.874×10^{-11}esu. All the third-order nonlinear properties were compared and reported in Table .7. The nonlinear absorption coefficient of present sample is reasonably larger than other chalcone derivatives and Terphenyl derivatives [55–57,58]. Similarly, third-order susceptibility is found to be two order higher than Terphenyl and methoxy based chalcone derivatives and comparable with other chalcone, dyes and Charge transfer complexes derivative materials [55–61]. The 3CP4NP shows better optical limiting response; hence, the nitro substituted chalcone derivative could be used for optical limiting application.

4. Conclusion

In the present contribution, nitro based chalcone derivative single crystal, grown by solvent evaporation technique is reported. The 3CP4NP belongs to noncentrosymmetric crystal system with $P2_1$ space group. The weak C–H···O interaction was the reason for crystal packing stability in the title compound. From UV-VIS-NIR study, the maximum absorbance was found to be 321 nm. Photoluminescence study reveals that, major defect states were obtained in the violet and blue region due to charge transfer effect. The presence of the nitro group in the molecule makes the crystal thermally stable up to 165 °C. From the theoretical calculation, the maximum polarizability is along y-direction($\alpha_{yy} = 39.42 \times 10^{-24} esu$) and first-order hyperpolarizability value is 48.3 times that of urea. Experimental result shows, SHG intensity value is very much smaller than that of KDP crystal. The low SHG efficiency is due to the charge transfer taking place at particular directions. The third-order nonlinear optical study proves that nonlinear response was improved with the substitution of nitro as an acceptor group and LDT value of 3CP4NP is found to be 7.34 GW/cm^2. Furthermore, optical limiting value and $\chi^{(3)}$ is found to be 0.59 GW/cm^2 and $8.74 \times 10^{-12} esu$. By suitable optimization, this chalcone material can be used for nonlinear optical applications.

Declaration of competing interest

The research paper entitled “Structural and optical characterization of novel nitro substituted D-π-A-π-A type chalcone single crystal showing second-order and third-order nonlinear optical properties” is not sent for publication in any other journal and is also not being under consideration for publication. The research subject is very much related and relevant to the scientific community working in the areas of materials science, physics and chemistry.

Acknowledgement

VP thanks to MAHE, Manipal for the financial assistance. The authors are thankful to Jayarama A., Alva’s Institute of Engineering and Technology, Moodbidri for extending support and Dr Poonam Tandon, University of Lucknow, Lucknow for theoretical studies. VP and ANP grateful to Dr. N. Sri Ram Gopal, University of Hyderabad, Hyderabad for experimental support (LDT-facility). ANP is thankful to Nagaraj K.K, MIT, Manipal and P.S. Patil, K.L.E. Institute of Technology, Hubballi for fruitful discussions. Authors are grateful to Dr P. K. Das, IISC, Bangalore, for SHG measurement.

References

[1] A.E. Whitten, D. Jayatilaka, M.A. Spackman, J. Chem. Phys. 125 (2006) 174505.
[2] G. de laTorre, P. Vazquez, F. Agullo-Lopez, T. Torres, Chem. Rev. 104 (2004) 3723–3750.
[3] D.S. Chemla, J. Zyss (Eds.), Non-Linear Optical Properties of Molecules and Crystals, Academic Press, New York, 1987.
[4] B. Zhang, G. Shi, Z. Yang, F. Zhang, S. Pan, Angew. Chem. Int. Ed. 56 (2017) 3916–3919.
[5] G. Shi, Y. Wang, F. Zhang, B. Zhang, Z. Yang, X. Hou, S. Pan, K.R. Poeppelmeier, J. Am. Chem. Soc. 139 (2017) 10645–10648.
[6] H.J. Ravindra, K. Chandrashekaran, W.T.A. Harrison, S.M. Dharmaprakash, Appl. Phys. B 94 (2009) 503–511.
[7] A. Gnoli, L. Razzari, M. Righini, Opt. Express 13 (2005) 7976–7981.
[8] G.S. He, C. Weder, P. Smith, P.N. Prasad, IEEE J. Quantum Electron. 34 (1998) 2279–2285.
[9] G.S. He, L.S. Tan, Q. Zheng, P.N. Prasad, Chem. Rev. 108 (2008) 1245–1330.
[10] P.A. Bouit, G. Wetzel, G. Berginc, B. Loiseaux, L. Toupet, P. Feneyrou, Y. Bretonniere, K. Kamada, O. Maury, C. Andraud, Chem. Mater. 19 (2007) 5325–5335.
[11] R.K. Saripalli, N.K. Katturi, V.R. Soma, H.L. Bhat, S. Elizabeth, J. Appl. Phys. 122 (2017) 223110.
[12] J.H. Jeong, B.J. Kang, J.S. Kim, M. Jazbinsek, S.H. Lee, S.C. Lee, I.H. Baek, H. Yun, J. Kim, Y.S. Lee, J.H. Lee, J.H. Kim, F. Rotermund, O.P. Kwon, Sci. Rep. 3 (2013) 1–8.
[13] S. Satheeshchandra, D. Haleshappa, S. Rohith, A. Jayarama, N. Shetty, Phys. B Condens. Matter 560 (2019) 191–196.

[14] E.D. D'silva, D. Narayan Rao, R. Philip, R.J. Butcher, Rajnikant, S. M. Dharmaprakash, Phys. B Condens. Matter 406 (2011) 2206–2210.
[15] C. Zhuang, W. Zhang, C. Sheng, W. Zhang, C. Xing, Z. Miao, Chem. Rev. 117 (2017) 7762–7810.
[16] E.D. Dsilva, D. Narayan Rao, R. Philip, R.J. Butcher, Rajnikant, S. M. Dharmaprakash, J. Phys. Chem. Solids 72 (2011) 824–830.
[17] J. Sun, G. Wang, C. Liu, Y. Shi, M. Zhao, Opt. Laser. Technol. 109 (2019) 600–607.
[18] P.P. Vinaya, A.N. Prabhu, K. Subrahmanya Bhat, V. Upadhyaya, Opt. Mater. 89 (2019) 419–429.
[19] A. Antony, S. Pramodini, I.V. Kityk, M. Abd-Lefdil, A. Douayar, F. Cherkaoui El Moursli, G. Sanjeev, K.B. Manjunatha, P. Poornesh, Phys. E Low-Dimensional Syst. Nanostructures. 94 (2017) 190–195.
[20] A.V. Uklein, V.V. Multian, G.M. Kuz'micheva, R.P. Linnik, V.V. Lisnyak, A.I. Popov, V.Y. Gayvoronsky, Opt. Mater. 84 (2018) 738–747.
[21] M. Frumar, B. Frumarova, T. Wagner, Compr. Semicond. Sci. Technol. 4 (2011) 206–261.
[22] A. Ekbote, P.S. Patil, S.R. Maidur, T.S. Chia, C.K. Quah, J. Mol. Struct. 1129 (2017) 239–247.
[23] T. Chandra Shekhara Shetty, S. Raghavendra, C.S. Chidan Kumar, S. Naveen, S. R. Maidur, P.S. Patil, S. Chandraju, G.S. Ananthnag, S.M. Dharmaprakash, Opt. Mater. 86 (2018) 138–147.
[24] A. Ekbote, P.S. Patil, S.R. Maidur, T.S. Chia, C.K. Quah, Dyes Pigments 139 (2017) 720–729.
[25] C. Shin, H. Lee, D.-R. Lee, C. Jung, D. Kim, B.K. Rhee, J. Korean Phys. Soc. 36 (2000) 356–359.
[26] B. Kulyk, B. Sahraoui, O. Krupka, V. Kapustianyk, V. Rudyk, E. Berdowska, S. Tkaczyk, I. Kityk, J. Appl. Phys. 106 (2009), 093102.
[27] S. tao Shi, Y. Fang, J. yi Yang, Y. bing Han, Y. lin Song, Opt. Mater. 86 (2018) 331–337.
[28] S. Raghavendra, C.S. Chidankumar, A. Jayarama, S.M. Dharmaprakash, Mater. Chem. Phys. 149 (2015) 487–494.
[29] S.R. Prabhu, A. Jayarama, K. Chandrasekharan, V. Upadhyaya, J. Mol. Struct. 1136 (2017) 244–252.
[30] A.N. Prabhu, A. Jayarama, K. Subrahmanya Bhat, V. Upadhyaya, J. Mol. Struct. 1031 (2013) 79–84.
[31] A. Kumar, R. Kumar, A. Gupta, P. Tandon, E.D. D'silva, J. Mol. Struct. 1150 (2017) 166–178.
[32] Bruker, APEX2, SAINT and SADABS, Bruker AXS Inc., Madison, WI, USA, 2009.
[33] G.M. Sheldrick, SHELXL-97 Program Automatic Solution of Crystal Structures, University of Göttingen: Go¨ttingen, Germany, 1997.
[34] G.M. Sheldrick, Acta Crystallogr. 71 (2015) 3–8.
[35] C.F. Macrae, I.J. Bruno, J.A. Chisholm, P.R. Edgington, P. McCabe, E. Pidcock, L. Rodriguez-Monge, R. Taylor, J. van de Streek, P.A. Wood, J. Appl. Crystallogr. 41 (2008) 466–470.
[36] J.M.F. Custodio, F.G. Santos, W.F. Vaz, C.E.P. Cunha, R.G. Silveira, M.M. Anjos, C. E.M. Campos, G.R. Oliveira, F.T. Martins, C.C. da Silva, C. Valverde, B. Baseia, H. B. Napolitano, J. Mol. Struct. 1157 (2018) 210–221.
[37] A. Praveen Menezes, A. Jayarama, S. Weng Ng, J. Cryst. Growth 402 (2014) 130–137.
[38] L.R. Almeida, M.M. Anjos, G.C. Ribeiro, C. Valverde, D.F.S. Machado, G. R. Oliveira, H.B. Napolitano, H.C.B. De Oliveira, New J. Chem. 41 (2017) 1744–1754.
[39] S. Raghavendra, C.S. Chidan Kumar, T.C.S. Shetty, B.N. Lakshminarayana, C. K. Quah, S. Chandraju, G.S. Ananthnag, R.A. Gonsalves, S.M. Dharmaprakash, Results Phys 7 (2017) 2550–2556.
[40] J.M.F. Custodio, G.D.C. D'Oliveira, F. Gotardo, L.H.Z. Cocca, L. De Boni, C. N. Perez, L.J.Q. Maia, C. Valverde, F.A.P. Osório, H.B. Napolitano, J. Phys. Chem. C 123 (2019) 5931–5941.
[41] P. Karuppasamy, T. Kamalesh, C. Senthil Kumar, M. Senthil Pandian, P. Ramasamy, S. Verma, S. Venugopal Rao, J. Mater. Sci. Mater. Electron. 30 (2019) 1553–1570.
[42] T. Chandra Shekhara Shetty, S. Raghavendra, C.S. Chidan Kumar, S. M. Dharmaprakash, Opt. Laser. Technol. 77 (2016) 23–30.
[43] N.L. Jadhav, A.B. Pandit, D.V. Pinjari, Sol. Energy 147 (2017) 232–239.
[44] S. Raghavendra, C.S. Dileep, S.M. Dharmaprakash, Structural , *Mol Cryst Liq Cryst.* 609 (2015) 192–204.
[45] P.P. Vinaya, A.N. Prabhu, K. Subrahmanya Bhat, V. Upadhyaya, J. Phys. Chem. Solids 123 (2018) 300–310.
[46] M.J. Frisch, G.W. Trucks, H.B. Schlegel, G.E. Scuseria, M.A. Robb, et al., Gaussian 09, Revision A. 02, Gaussian, Inc., Wallingford CT, 2010.
[47] A.D. Becke, J. Chem. Phys. 98 (1993) 5648–5652.
[48] G.A. Petersson, A. Bennett, T.G. Tensfeldt, M.A. Al-Laham, W.A. Shirley, J. Mantzaris, J. Chem. Phys. 89 (1988) 2193–2218.
[49] D.A. Kleinman, Phys. Rev. 126 (1962) 1977–1979.
[50] C. Adant, M. Dupuis, J.L. Bredas, Int. J. Quantum Chem. 56 (1995) 497–507.
[51] M. Nakano, S. Kiribayashi, S. Yamada, I. Shigemoto, K. Yamaguchi, Chem. Phys. Lett. 262 (1996) 66–73.
[52] S.K. Kurtz, T.T. Perry, J. Appl. Phys. 39 (1968) 3798.
[53] M. Sheik-Bahae, A.A. Said, T.H. Wei, D.J. Hagan, E.W. V Stryland, IEEE J. Quantum Electron. 26 (1990) 760–769.
[54] M. Sheik-Bahae, A.A. Said, E.W.V. Stryland, Opt. Lett. 14 (1989) 955–957.
[55] A.N. Prabhu, V. Upadhyaya, A. Jayarama, K. Subrahmanya Bhat, Mater. Chem. Phys. 138 (2013) 179–185.
[56] T.C. Shekhara, C.S.C. Kumar, K.N.G. Patel, T. Shyang, S.M. Dharmaprakash, P. Ramasami, Y. Umar, S. Chandraju, C. Kheng, J. Mol. Struct. 1143 (2017) 306–317.
[57] H.J. Ravindra, A. John Kiran, K. Chandrasekharan, H.D. Shashikala, S. M. Dharmaprakash, Appl. Phys. B 88 (2007) 105–110.
[58] L. Kamath, K.B. Manjunatha, S. Shettigar, G. Umesh, B. Narayana, S. Samshuddin, B.K. Sarojini, Opt. Laser. Technol. 56 (2014) 425–429.
[59] P.S. Patil, S.R. Maidur, S. Venugopal Rao, S.M. Dharmaprakash, Opt. Laser. Technol. 81 (2016) 70–76.
[60] M.C. Sreenath, I. Hubert Joe, V.K. Rastogi, Opt. Laser. Technol. 108 (2018) 218–234.
[61] M.C. Divyasree, K. Vasudevan, K.K. Abdul Basith, P. Jayakrishnan, M.T. Ramesan, K. Chandrasekharan, Opt. Laser. Technol. 105 (2018) 94–101.